

Recursive-ARX for Grid-Edge Fault Detection

Soufiane El Yaagoubi,^{*} Keith Moffat,[†]
Eduardo Prieto Araujo,^{*} Florian Dörfler[†]

^{*}CITCEA, Polytechnic University of Catalonia, Barcelona, Spain

Emails: soufielyaagoubi@gmail.com, eduardo.prieto-araujo@upc.edu

[†]Automatic Control Laboratory, Swiss Federal Institute of Technology (ETH), Zürich, Switzerland

Emails: kmoffat@ethz.ch, dorfler@ethz.ch

Abstract—Future electrical grids will require new ways to identify faults as inverters are not capable of supplying large fault currents to support existing fault detection methods and because distributed resources may feed faults from the edge of the grid. This paper proposes the use of real-time system identification for online power-system fault detection. Specifically, we implement Recursive ARX (rARX) system identification on a grid-connected inverter. Experiments demonstrate that the proposed rARX method is able to both detect large faults quickly, and distinguish between high-impedance faults and large load increases. These results indicate that rARX grid-edge fault detection is a promising research direction for improving the reliability and safety of modern electric grids.

Index Terms—Grid-Edge, Fault Detection, Online, ARX System Identification, Grid-Connected Inverters.

I. INTRODUCTION

As inverters continue to replace synchronous generators, traditional fault-detection and protection methods for electric grids may become insufficient as 1) inverters are not capable of supplying large fault currents to support existing fault detection methods, 2) distributed, grid-edge resources transition from grid-following to grid-forming operation [1], and thus distributed resources may feed faults from the edge of the grid, and 3) high-impedance faults (HIFs), which can ignite fires, can be difficult to distinguish from large load increases.

HIFs have become a particularly important challenge in arid environments in which faults can lead to large wildfires. HIFs occur when a distribution network conductor comes into contact with an object such as a tree or a pole that provides a high-impedance path to ground. As the resulting fault current can be lower than the nominal max current at the fault location [2], conventional protection systems have a difficult time detecting the HIF and tripping the relay [3]. Studies indicate that approximately/at least 20% of the faults in distribution systems are HIFs [4], [5].

Fig. 2 provides a classification scheme for Fault Detection and Diagnosis (FDD), dividing the methods into model-based or data-driven methods categories. Model-based approaches are either quantitative and qualitative models [6]. While these methods can be powerful, they require extensive system-specific modeling and knowledge, making them impractical in many real-world applications [7].

This research is supported by the Swiss National Science Foundation under the NCCR Automation (grant agreement 51NF40_180545)

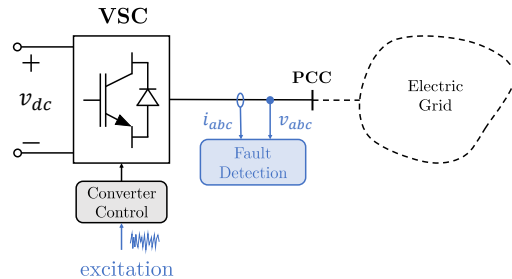


Fig. 1. Data-Driven Grid-edge Fault Detection

In contrast, data-driven methods are divided into process history-based and model-free rule-based approaches [6]. Model-free rule-based methods, such as limit-checking and trend analysis, provide a simple fault detection strategy based on predefined thresholds such as voltage lower-limits. While these methods are sufficient for detecting low-impedance faults (LIFs) [8], they can fail to detect HIFs.

Process history-based methods are further categorized into black-box and grey-box models [6]. Grey-box models incorporate some physics-based knowledge, while black-box models do not. Black-box models require only input/output data to identify faults by deriving patterns from the data, and thus provide a flexible, plug-and-play fault identification solution. The literature contains both neural network-based approaches [9], [10] and statistics-based system identification approaches. Statistical approaches, which consider the noise characteristics of an underlying process and are optimal in some way, have been used for fault detection in a number of applications such as HVAC [11] and Lithium-ion battery systems [12], [13].

This paper proposes rARX grid-edge fault detection based on the insight that faults change grid dynamics. That is, if a fault occurs in the system, the dynamic relation between the current injections at a point on the grid edge and the voltage measured at that point will change. The rARX algorithm identifies time-domain parameters, similar to [14], that are monitored to detect if the system dynamics have changed. Our hypothesis, tested in this paper, is that rARX system identification can both detect LIFs quickly using no model information (black-box), and distinguish between HIFs and load increases based on specific parameters (grey-box).

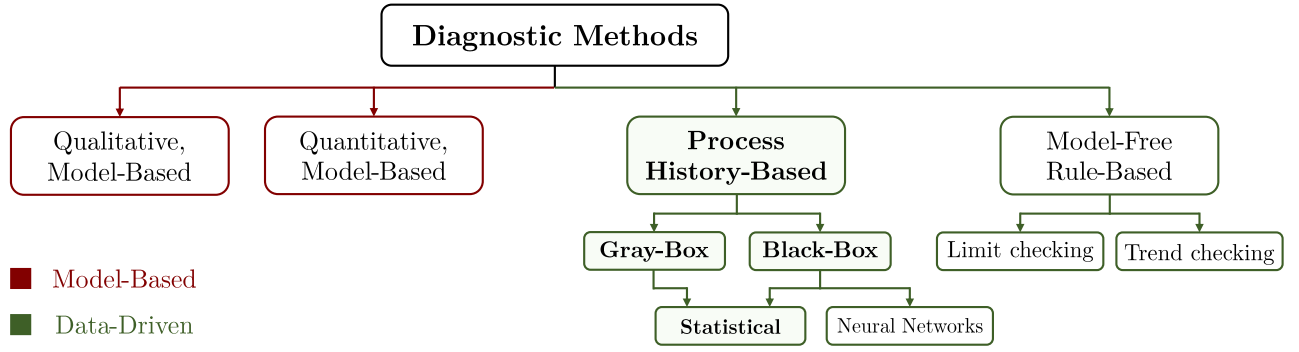


Fig. 2. Classification scheme for FDD methods.

This paper is organized as follows: Section II provides the necessary background. Section III presents the fault detection approach. Section IV validates the method through simulations and comparisons and Section V concludes the paper.

II. BACKGROUND

A. ARX System Identification

We consider a time-domain ARX model of a system with combined input and output dimension l . The set of measurements for ρ steps into the past at time k are collected into the data regressor $\varphi(k) \in \mathbb{R}^{l\rho}$,

$$\varphi(k) = [y(k-1)^\top \cdots y(k-\rho)^\top \ u(k-1)^\top \cdots u(k-\rho)^\top]^\top.$$

The dynamics model for a one-dimensional output is

$$y(k) = \theta\varphi(k) + \epsilon(k), \quad (1)$$

where $\theta \in \mathbb{R}^{1 \times l\rho}$ is the predictor matrix and $\epsilon(k)$ is the white noise innovation [15].

The batch least-squares estimate of θ at timestep k minimizes the cost function

$$\mathcal{J}_N(k) = \sum_{i=1}^N \|y(k-i) - \theta\varphi(k-i)\|^2$$

for some data window-length N . Instead, we implement the Recursive ARX (rARX) algorithm, which estimates $\theta(k)$, the predictor at timestep k , based on the exponential forgetting factor $\lambda \in (0, 1]$:

$$\mathcal{J}_\infty(k) = \sum_{i=0}^{\infty} \lambda^i \|y(k-i) - \theta(k)\varphi(k-i)\|^2. \quad (2)$$

$\mathcal{J}_\infty(k)$ prioritizes recent measurements more than $\mathcal{J}_N(k)$, and thus is better suited for fault detection applications for which speed-of-detection is important. The forgetting factor can be chosen explicitly, or updated automatically based on data [12]. Given the Kalman gain $K \in \mathbb{R}^{l\rho}$ at time k ,

$$K(k) = \frac{P(k-1)\varphi(k)}{\lambda + \varphi(k)^\top P(k-1)\varphi(k)},$$

calculated using the recursively-calculated covariance of $\theta(k)$,

$$P(k) = \frac{1}{\lambda} (P(k-1) - K(k)\varphi(k)^\top P(k-1)),$$

the recursively-calculated

$$\theta(k) = \theta(k-1) + (y(k) - \theta(k-1)\varphi(k))K(k)^\top \quad (3)$$

minimizes $\mathcal{J}_\infty(k)$ [15].

B. Converter Data Preprocessing

For grid-edge system identification, as shown in Fig. 1, we define the input as the current injected into the grid at the PCC, and the output as the voltage measured at the PCC. The three-phase $v_{abc}(k)$ and $i_{abc}(k)$ signals are converted to dq reference-frame signals using the frequency measured locally by the converter's Phase-Locked-Loop (PLL). The inputs and outputs used for the small-signal system identification are the time-difference signals

$$u(k) = \Delta i_{dq}(k) = i_{dq}(k) - i_{dq}(k-1) \in \mathbb{R}^2, \text{ and} \\ y(k) = \Delta v_{dq}(k) = v_{dq}(k) - v_{dq}(k-1) \in \mathbb{R}^2.$$

To ensure persistency of excitation, we add random binary sequence (RBS) noise to the output of the converter's current-control loop.

III. RECURSIVE ARX FOR FAULT DETECTION

This section describes the grid-edge fault detection method that we propose in this paper. The rARX algorithm estimates the grid parameters at each time step k and a fault is detected if the parameters vary significantly. The predictor for $y_d(k) = \Delta v_d(k)$ is $\theta_d(k)$, and the predictor for $y_q(k) = \Delta v_q(k)$ is $\theta_q(k)$:

$$\Delta v_d(k) = \theta_d(k)\varphi(k) + \epsilon_d(k), \text{ and} \\ \Delta v_q(k) = \theta_q(k)\varphi(k) + \epsilon_q(k).$$

$\theta_d(k)$ and $\theta_q(k)$ are vertically-concatenated to give

$$\boldsymbol{\theta}(k) = \begin{bmatrix} \theta_d(k) \\ \theta_q(k) \end{bmatrix} \in \mathbb{R}^{2 \times 4\rho}.$$

The algorithm we propose, described in Fig. 3 and Algorithm 1, consists of two criteria. Both criteria use the deviation of $\boldsymbol{\theta}(k)$ from $\boldsymbol{\theta}^*$, the nominal output predictor that was obtained at some point in the past at which the system was operating with no faults present.

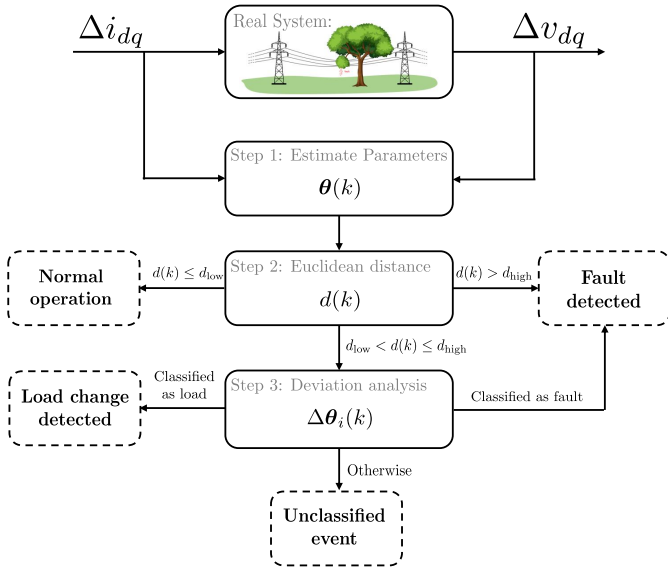


Fig. 3. Proposed method for detecting faults.

The first, Euclidian-distance criterion, based on

$$d(k) = \|\theta(k) - \theta^*\|_F,$$

($\|\cdot\|_F$ denotes the Frobenius Norm) checks for large (high-admittance) faults, which change the output predictor parameters significantly. The Euclidian-distance criterion uses d_{high} , which is determined by running experiments and/or simulations offline.

The second criterion is triggered if $d_{\text{low}} < d(k) \leq d_{\text{high}}$, and is designed to catch HIFs. The intuition for the second criterion is that the introduction of a resistive path to ground (used to model a HIF), and an inductive path to ground (used to model an inductive load increase such as a motor-start), will produce different dynamics. This intuition is demonstrated with specific circuit parameters in Appendix A. The parameters identified by the rARX model indicate which set of dynamics is present in the system. Standard low-voltage limit-checking methods are not able to make the same distinction.

To differentiate between HIFs and large load increases, each

$$\begin{aligned} \Delta\theta_{d,i}(k) &= \theta_{d,i}(k) - \theta_{d,i}^* \text{ and} \\ \Delta\theta_{q,i}(k) &= \theta_{q,i}(k) - \theta_{q,i}^* \end{aligned}$$

is analyzed individually (i indicates the index of the component in the $\Delta\theta_d$ or $\Delta\theta_q$ vector). The deviation of each vector component is compared with a library of known faults and large load-increase behaviors, providing the basis for the fault/no fault decision. The library is built by running experiments and/or simulations offline. As this portion of the method requires system information (i.e., a simulator), it is grey-box rather than black-box.

IV. SIMULATION VALIDATION & COMPARISON

To validate our proposed rARX for fault detection and compare it with current methods, we use Simscape Electrical

Algorithm 1 Fault Detection Algorithm

Initialization:

Set nominal parameters θ^* using fault-free system data

Set thresholds d_{high} , d_{low} and the forgetting factor λ

for each time step k **do**

Estimate parameters $\theta(k)$

Compute Euclidean distance: $d(k)$

if $d(k) > d_{\text{high}}$ **then**

Fault detected

else if $d(k) > d_{\text{low}}$ **then**

Compare $\Delta\theta_{d,i}$ and $\Delta\theta_{q,i}$ with recorded cases

if Deviation matches a fault case **then**

Fault detected

else if Deviation matches a load increase case **then**

Load increase detected

else

Unclassified event

end if

else

Normal operation

end if

end for

in MATLAB/Simulink to perform electromagnetic transient (EMT) simulations. The electrical parameters are provided in Table I.

Fig. 4 describes the circuit used for the tests. This circuit includes an electrical network line with load R_1, C_1 and a Thevenin-equivalent model of the grid, which includes an infinite bus and the impedances R_2, L_2, R_3 , and L_3 . The impedance Z_i is activated at t_{start} and deactivated at t_{end} and is either a fault or a load, depending the test being run. In the case of a fault, $Z_i = R_{\text{fault}}$ and, in the case of a load increase, $Z_i = jX_{\text{load}}$, where $X_{\text{load}} = \omega_g L_{\text{load}}$. We add two uncorrelated RBS signals to the output of the current controller to provide system excitation, each with an amplitude of 0.1 p.u. and a sampling frequency of 5 kHz into the control loop of the converter, as shown in Fig. 4. $\rho = 3$ was chosen for the ARX model as it results in an R^2 coefficient of determination [17] below 5%, providing a good fit to the model while not over-parameterizing for the training data.

TABLE I
ELECTRICAL PARAMETERS OF THE NUMERICAL EXPERIMENT.

Parameter	Symbol	Value
Voltage, power, & freq. base	V_b, S_b, f_b	380 V, 1.5 kVA, 50 Hz
LCL filter components	L_{f1}, L_{f2}, C_f	0.08 p.u., 0.05 p.u., 0.08 p.u.
Load component	R_1, C_1	2 p.u., 0.05 p.u.
Line 1	R_2, L_2	0.015 p.u., 0.15 p.u.
Line 2	R_3, L_3	0.015 p.u., 0.15 p.u.

A. Demonstration of the Proposed rARX Method

1) *rARX for LIF detection*: To demonstrate the operation of the proposed method for a LIF, a simulation is carried out in which a LIF ($R = 20\Omega$) is active from $t_{\text{start}} = 10$ s to $t_{\text{end}} = 20$ s. Fig. 5 illustrates how the parameter vector

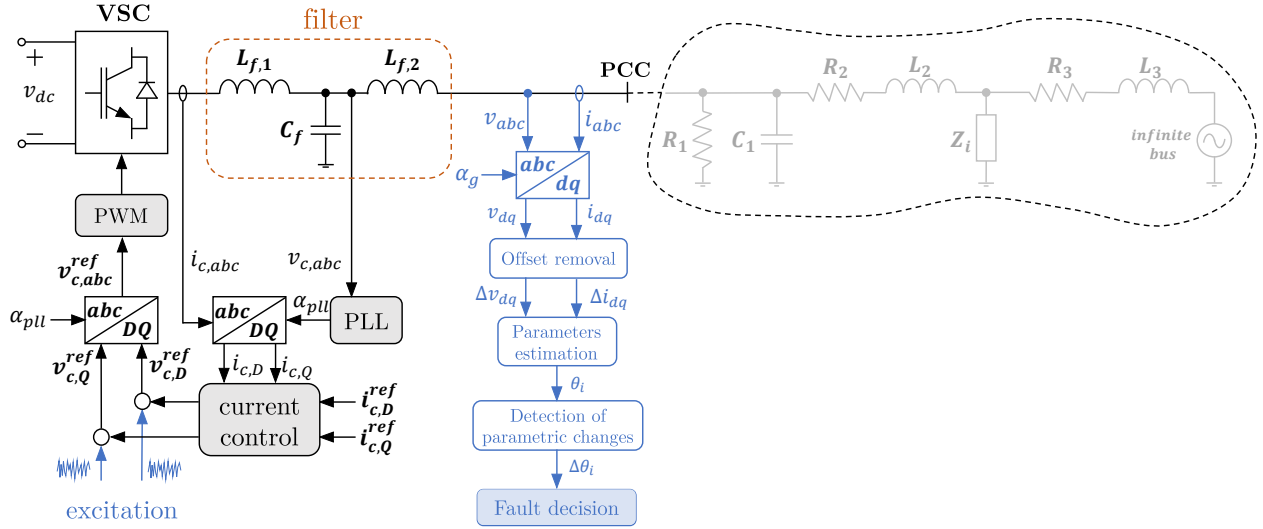


Fig. 4. Fault-detection simulation set-up

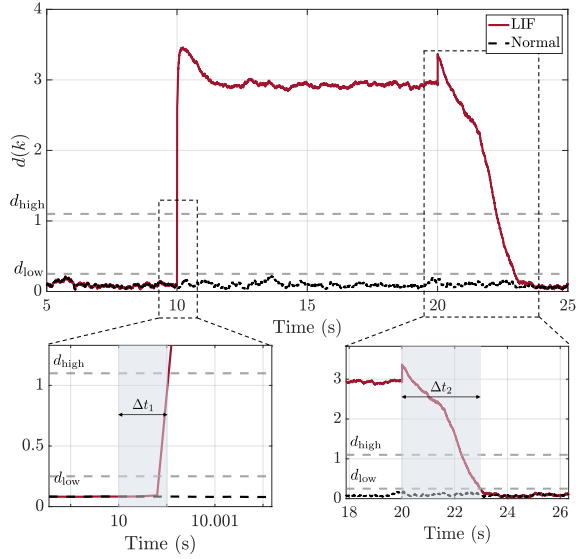


Fig. 5. Low-impedance fault (LIF) test

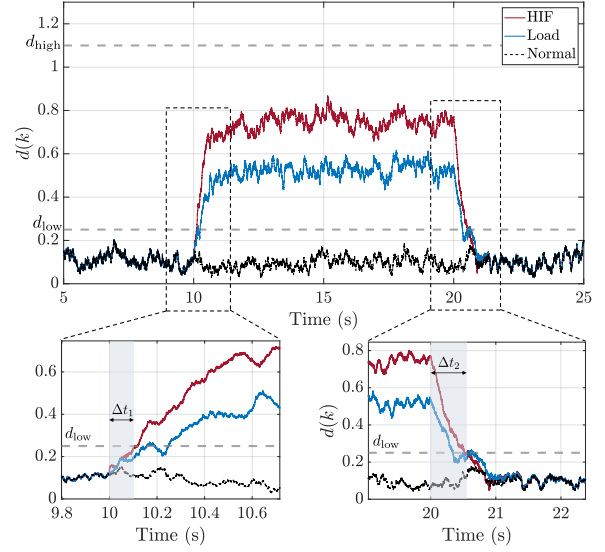


Fig. 6. High-impedance fault (HIF) test

distance $d(k)$ varies with time for the LIF. $\Delta t_1 = 0.0005s$ is the time elapsed from t_{start} until $d(k) > d_{high}$, and $\Delta t_2 = 2.9s$ is the time from t_{end} until $d(k) \leq d_{low}$. While noting that these detection times are dependent upon the forgetting factor parameter λ and therefore can be easily increased/decreased, the $\Delta t_1 = 0.0005s$ fault detection time for the given parameters is promising.

2) *rARX for HIF detection*: To demonstrate the operation of the proposed method for a HIF, two simulations are carried out, one with a HIF, and one with a load increase. The HIF and the load increase are active from $t_{start} = 10s$ to $t_{end} = 20s$.

Fig. 6 illustrates how the parameter vector distance $d(k)$ varies with time for the HIF. $\Delta t_1 = 0.10s$ is the time elapsed from t_{start} until $d(k) > d_{low}$, and $\Delta t_2 = 0.6s$ is

the time from t_{end} until $d(k) \leq d_{low}$. Once again, these detection times are dependent upon the forgetting factor parameter λ , which may be adjusted as necessary. The parameter-specific/recorded-cases criterion in Algorithm 1 is activated when $d_{low} < d(k) \leq d_{high}$, which is illustrated in Fig. 7. The significant differences between parameter estimates when a (resistive) HIF has occurred and when an (inductive) load increase has occurred demonstrate the viability of rARX for detecting HIFs.

B. Comparison to Voltage Limit-Checking

Voltage limit-checking is the de-facto standard for grid-edge fault detection. The limit-checking method can be applied in

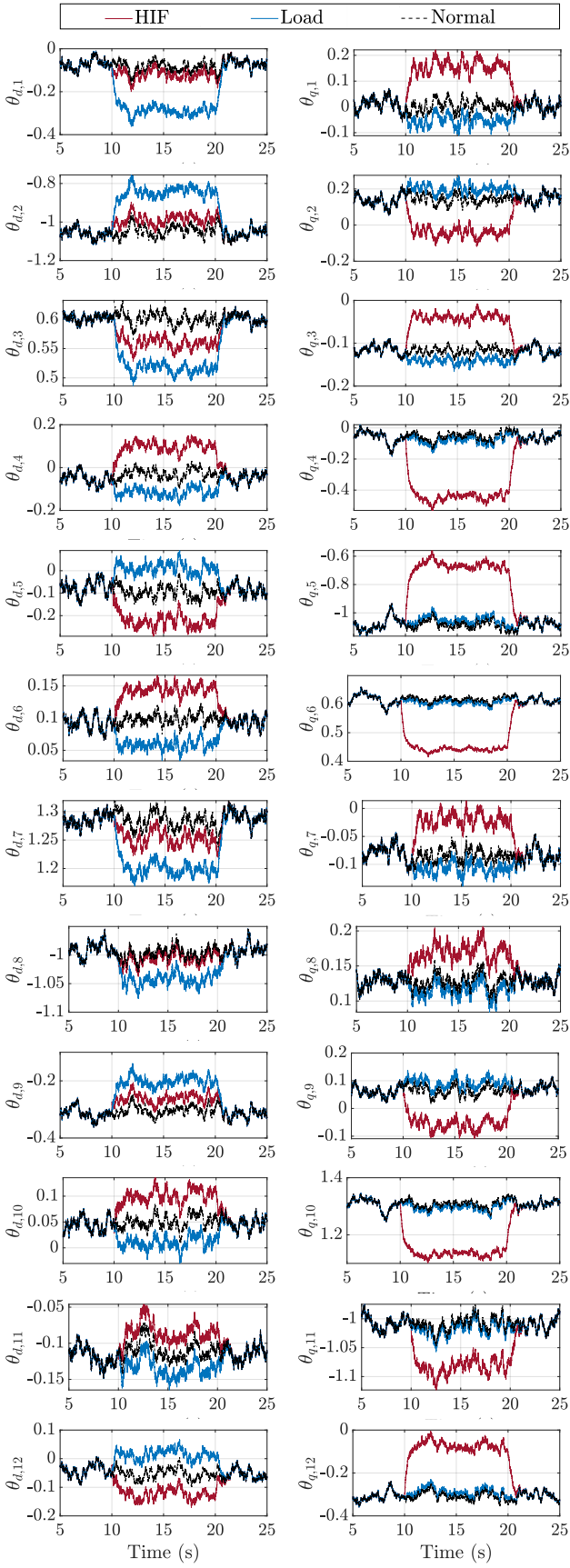


Fig. 7. Parameters for the high-impedance fault test

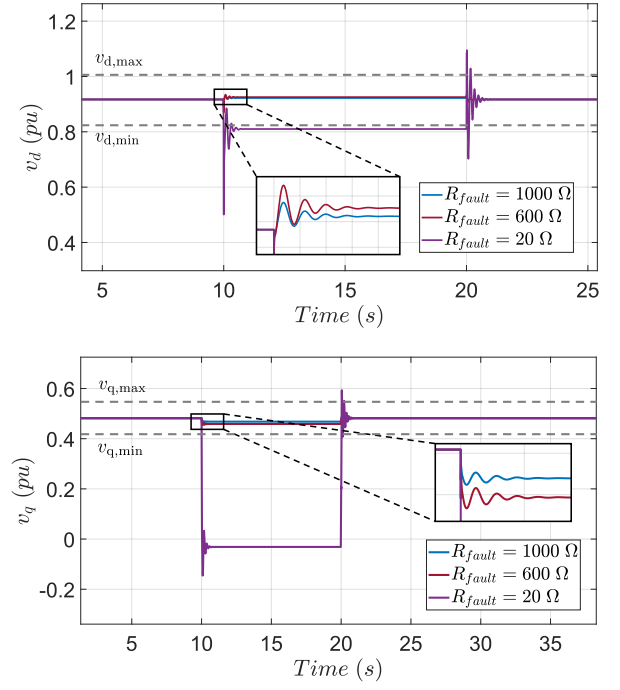


Fig. 8. Demonstration of limit-checking for faults with three different resistance values

the dq -reference frame using the following user-defined limits:

$$\begin{aligned} v_{d,\min} < v_d(k) < v_{d,\max} \\ v_{q,\min} < v_q(k) < v_{q,\max} \end{aligned} \quad (4)$$

Fig. 8 shows how v_d and v_q vary for different values of R_{fault} . It is evident that when the fault resistance is low, i.e. $R_{\text{fault}} = 20 \Omega$, the limit-checking method can easily detect the fault. However when the fault resistance is high, i.e. $R_{\text{fault}} = 600 \Omega$ or $R_{\text{fault}} = 1000 \Omega$, the limit-checking method cannot detect the fault. Thus, the parameter-specific test in Step 3 of our method (Fig. 3) is well motivated.

V. CONCLUSION

This paper presented a novel approach for real-time fault detection in power grids using rARX. The proposed method continuously updates system parameters and detects faults by evaluating deviations from the nominal model. The algorithm follows a two-step decision-making process: first, it detects anomalies based on parameter deviations, and second, it distinguishes between grid faults and inductive load increases by analyzing the specific parameters.

The results in this paper indicate that rARX grid-edge fault detection is a promising research direction. Future research directions include developing a method for building the fault-vs.-load-increase parameter dictionary, which is necessary for reliably detecting high-impedance faults, and increasing the speed of the fault detection by using methods such as optimal forgetting factors and excitation design.

REFERENCES

- [1] R. H. Lasseter, Z. Chen and D. Pattabiraman, "Grid-Forming Inverters: A Critical Asset for the Power Grid," *IEEE Journal of Emerging and Selected Topics in Power Electronics*, vol. 8, no. 2, pp. 925-935, June 2020.
- [2] M. Wei, W. Liu, H. Zhang, F. Shi and W. Chen, "Distortion-Based Detection of High Impedance Fault in Distribution Systems," *IEEE Transactions on Power Delivery*, vol. 36, no. 3, pp. 1603-1618, June 2021.
- [3] El Sayed Tag Eldin, D. k. Ibrahim, E. M. Aboul-Zahab and S. M. Saleh, "High Impedance Faults Detection in EHV Transmission Lines Using the Wavelet Transforms," *2007 IEEE Power Engineering Society General Meeting*, Tampa, FL, USA, 2007, pp. 1-7.
- [4] A. Soheilil and J. Sadeh, "Evidential reasoning based approach to high impedance fault detection in power distribution systems," *IET Generation, Transmission and Distribution*, vol. 11, no. 5, pp. 1325-1336, Mar. 2017.
- [5] S. Mondal and R. Pradhan, "A critical analysis on different high impedance fault detection schemes," *Electric Power Components and Systems*, 2023.
- [6] S. Katipamula and M. R. Brambley, "Methods for fault detection, diagnostics, and prognostics for building systems: A review, part I," *HVAC&R Research*, vol. 11, no. 1, pp. 3-25, 2005.
- [7] A. Beghi, R. Brignoli, L. Cecchinato, G. Menegazzo, M. Rampazzo and F. Simmini, "Data-driven fault detection and diagnosis for HVAC water chillers," *Control Engineering Practice*, vol. 53, pp. 79-91, 2016.
- [8] N. Praisuwanana, L. M. Tolbert, J. Wang and F. Li, "Fault Detection Method by Utilizing Instantaneous Power Theory for Inverter-based Distributed Generation,"
- [9] S. Heo and J. H. Lee, "Fault detection and classification using artificial neural networks," *IFAC-PapersOnLine*, vol. 51, no. 18, pp. 470-475, 2018.
- [10] F. Lv, C. Wen, Z. Bao and M. Liu, "Fault diagnosis based on deep learning," *2016 American Control Conference (ACC)*, Boston, MA, USA, 2016, pp. 6851-6856.
- [11] W. J. N. Turner, A. Staino and B. Basu, "Residential HVAC fault detection using a system identification approach," *Energy and Buildings*, vol. 151, pp. 1-17, 2017.
- [12] X. Sun et al., "Adaptive forgetting factor recursive least square algorithm for online identification of equivalent circuit model parameters of a lithium-ion battery," *Energies*, vol. 12, no. 11, June 2019.
- [13] E. Din, C. Schaef, K. Moffat and J. T. Stauth, "A Scalable Active Battery Management System With Embedded Real-Time Electrochemical Impedance Spectroscopy," *IEEE Transactions on Power Electronics*, vol. 32, no. 7, pp. 5688-5698, July 2017.
- [14] V. Haberle, L. Huang, X. He, E. Prieto-Araujo, R. S. Smith and F. Dorfler, "MIMO Grid Impedance Identification of Three-Phase Power Systems: Parametric vs. Nonparametric Approaches," *2023 62nd IEEE Conference on Decision and Control (CDC)*, Singapore, Singapore, 2023, pp. 542-548.
- [15] L. Ljung, "System Identification: Theory for the User," *Prentice Hall*, 1997.
- [16] L. Harnefors, "Modeling of Three-Phase Dynamic Systems Using Complex Transfer Functions and Transfer Matrices," *IEEE Transactions on Industrial Electronics*, vol. 54, no. 4, pp. 2239-2248, Aug. 2007.
- [17] D. Chicco, M.J. Warrens, G. Jurman, "The coefficient of determination R-squared is more informative than SMAPE, MAE, MAPE, MSE and RMSE in regression analysis evaluation," *PeerJ Comput Sci*, 2021.

APPENDIX A

MODEL-BASED INTUITION FOR DIFFERENTIATING BETWEEN HIFs AND INDUCTIVE LOAD INCREASES

This Appendix describes how the poles of the small-signal grid model depend on whether the introduced disturbance is an HIF or an inductive load. The purpose is to demonstrate that, given sufficient data, an rARX model should be able to distinguish between an HIF and an inductive load. The grid model is taken from the converter's perspective, at the point of common coupling, as shown in Fig. 4. For simplicity, we remove R_1 and C_1 , producing the circuit in Fig. 9.

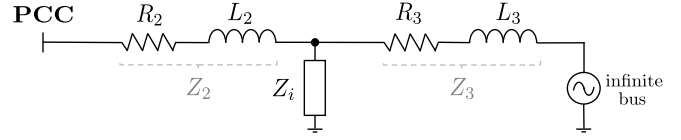


Fig. 9. Equivalent circuit with a fault and a load increase.

The small-signal dq grid impedance, $Z_g(s)$, relates the terminal voltages to the currents at the PCC at the steady-state grid frequency ω_g . $Z_g(s)$ consists of four transfer functions: $Z_{g,dd}(s)$, $Z_{g,qd}(s)$, $Z_{g,dq}(s)$, and $Z_{g,qq}(s)$, such that [16]

$$\begin{bmatrix} \Delta v_d(s) \\ \Delta v_q(s) \end{bmatrix} = \begin{bmatrix} Z_{g,dd}(s) & Z_{g,qd}(s) \\ Z_{g,dq}(s) & Z_{g,qq}(s) \end{bmatrix} \begin{bmatrix} \Delta i_d(s) \\ \Delta i_q(s) \end{bmatrix}.$$

The grid impedance before the fault is

$$Z_{g,\text{nom}}(s) = Z_2(s) + Z_3(s),$$

where

$$Z_2(s) = \begin{bmatrix} R_2 + sL_2 & -\omega_g L_2 \\ \omega_g L_2 & R_2 + sL_2 \end{bmatrix}$$

and

$$Z_3(s) = \begin{bmatrix} R_3 + sL_3 & -\omega_g L_3 \\ \omega_g L_3 & R_3 + sL_3 \end{bmatrix}.$$

After the disturbance, the grid impedance is

$$Z_{g,\text{post}}(s) = (Z_3^{-1}(s) + Z_i^{-1})^{-1} + Z_2(s).$$

where Z_i is either Z_{fault} or Z_{load} .

As HIFs typically occur when a conductor comes into contact with a short-but-high-resistance path to ground, we approximate

$$Z_{\text{fault}}(s) = \begin{bmatrix} R_{\text{fault}} & 0 \\ 0 & R_{\text{fault}} \end{bmatrix}.$$

The poles for each of the four transfer functions after the fault, obtained with the parameters in Table I, are

$$s_{1,2,\text{fault}} = -\frac{20}{3}R_{\text{fault}} - \frac{1}{10} \pm j.$$

We focus on differentiating HIFs from inductive load increases, such as a motor start or the connection/reclosing of a transformer to a distribution network. The inductive load increase in complex coordinates is $Z_{\text{load}} = jX_{\text{load}}$, where $X_{\text{load}} = \omega_g L_{\text{load}}$, and in dq coordinates is

$$Z_{\text{load}}(s) = \begin{bmatrix} sL_{\text{load}} & -\omega_g L_{\text{load}} \\ \omega_g L_{\text{load}} & sL_{\text{load}} \end{bmatrix}.$$

The poles for each of the four transfer functions after a load increase, obtained with the same parameter values, are

$$s_{1,2,\text{load}} = \frac{-3}{200L_{\text{load}+30}} \pm j.$$

As $s_{1,2,\text{fault}} \neq s_{1,2,\text{load}}$, we expect that, given sufficient data, an rARX model should be able to distinguish between an HIF and an inductive load.